Reward Finetuning for Faster and More Accurate Unsupervised Object Discovery

Katie Z Luo*1,† Zhenzhen Liu*1 Xiangyu Chen*1 Yurong You¹ Sagie Benaim² Cheng Perng Phoo¹
Mark Campbell¹ Wen Sun¹ Bharath Hariharan¹ Kilian Q. Weinberger¹

¹Cornell University, Ithaca, NY ²The Hebrew University of Jerusalem

Abstract

Recent advances in machine learning have shown that Reinforcement Learning from Human Feedback (RLHF) can improve machine learning models and align them with human preferences. Although very successful for Large Language Models (LLMs), these advancements have not had a comparable impact in research for autonomous vehicles—where alignment with human expectations can be imperative. In this paper, we propose to adapt similar RL-based methods to unsupervised object discovery, i.e. learning to detect objects from LiDAR points without any training labels. Instead of labels, we use simple heuristics to mimic human feedback. More explicitly, we combine multiple heuristics into a simple reward function that positively correlates its score with bounding box accuracy, i.e., boxes containing objects are scored higher than those without. We start from the detector's own predictions to explore the space and reinforce boxes with high rewards through gradient updates. Empirically, we demonstrate that our approach is not only more accurate, but also orders of magnitudes faster to train compared to prior works on object discovery. Code is available at https://github.com/katieluo88/DRIFT.

1 Introduction

Self-driving cars need to accurately detect the moving objects around them in order to move safely. Most modern 3D object detectors rely on supervised training from 3D bounding box labels. However, these 3D bounding box labels are hard to acquire from human annotation. Furthermore, this supervised approach relies on a pre-decided vocabulary of classes, which can cause problems when the car encounters novel objects that were never annotated.

Our prior work, MODEST [55], introduced the first method to train 3D detectors without labeled data. In that work, we point out that instead of specifying millions of labels, one can succinctly describe heuristics for what a good detector output should look like. For example, one can specify that detector boxes should mostly enclose transient foreground points rather than background ones; they should roughly be of an appropriate size; their sides should be aligned with the LiDAR points; their bottom should touch the ground, etc. Although such heuristics are great for scoring a set of boxes proposed by a detector, training a detector on them is hard for two reasons: First, these heuristics are often non-linear, non-differentiable functions of the detector parameters (for example, a slight shift of the box can cause all foreground points to fall off.) Second, existing object detection pipelines use carefully designed training objectives that heavily rely on labeled boxes, that are difficult to modify (for example, PointRCNN [40] infers point labels from box labels and uses these for training). For these reasons, MODEST had to utilize an admittedly slow self-training pipeline to incrementally incorporate common-sense heuristics.

^{*}Denotes equal contribution.

[†]Correspondences could be directed to kzl6@cornell.edu

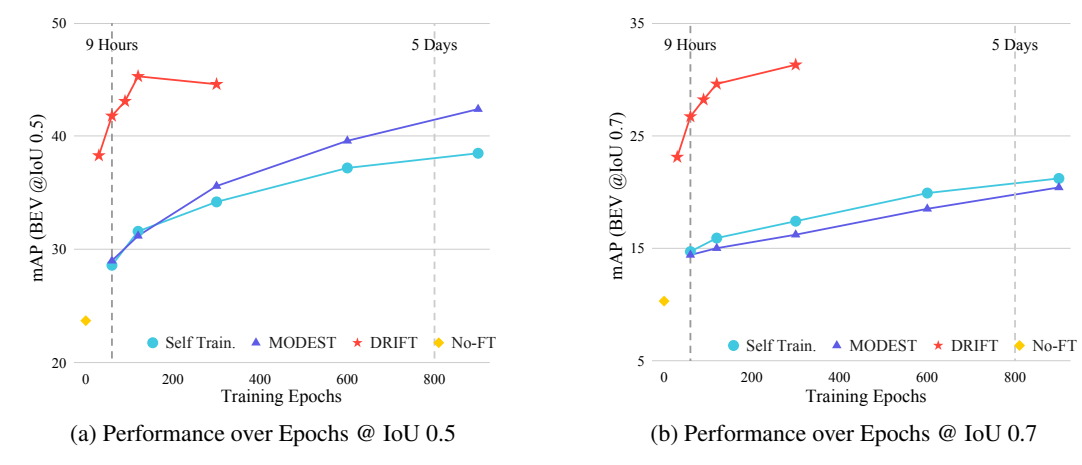


Figure 1: **Detection performance on Lyft test data as a function of training epochs.** DRIFT demonstrates significantly stronger performance and faster learning. With only 9 hours of training, it outperforms both baselines that have been trained for days.

In this paper, we propose a new reward ranking based framework that utilizes these common-sense heuristics directly as a reward signal. Our method relies on finetuning with reward ranking [31, 27, 13, 33], where given an initialized object detector, we finetune it for a predefined set of desirable detection properties. This bypasses the need to encode heuristics as differentiable loss functions and avoids the need to hand-engineer training paradigms for each kind of object detector. Recent success with reinforcement learning from human feedback (RLHF) has proven effective in improving machine learning models —in particular, large language models (LLMs)— and aligning them with human preferences [31, 27]. However, these advancements have not been applicable to detection-based vision models that are trained with per-instance regression and are difficult to view under a probabilistic framework. To address this challenge, we utilize insights from reward ranked finetuning [13], a non-probabilistic paradigm designed for finetuning of LLMs, which inspired us to develop a similar framework for object discovery.

We refer to our method as *Discovery from Reward-Incentivized Finetuning (DRIFT)*. DRIFT does not require labels, and instead uses the Persistency Prior (PP) score [55, 3] as a heuristic to identify dynamic foreground points based on historical traversals. These foreground points give rise to rough (and noisy) label estimates [55], which we use to pre-train our detector. The resulting detector performs poorly but suffices to propose many boxes of roughly the right sizes that we can use for exploration. To facilitate reward ranked finetuning, we first propose a reward function to score boxes. Ideally, only boxes that tightly contain objects (e.g. a car) should yield high rewards. We achieve this by combining several simple heuristics (e.g. high ratio of foreground points) and assuming some rough knowledge about the object dimensions. During each iteration of training, DRIFT performs the following steps: 1. the object detector proposes many boxes in a given point cloud scene; 2. the boxes are "jittered" through random perturbations (as a means of exploration); 3. the boxes are scored according to the reward function; 4. the top-k% non-overlapping boxes are kept as pseudo-labels for gradient updates.

We evaluate DRIFT on two large, real-world datasets [12, 24] and show that we significantly outperform prior self-training methods both in efficiency and generalizability. Experimental results demonstrate that using reward ranked finetuning for object discovery under our framework can quickly converge to a solution that is on par with out-of-domain supervised object detectors within a few training epochs, suggesting that DRIFT may point towards a more general unsupervised learning formulation for object detectors in an in-the-wild setting.

2 Related Works

3D Object Detection. 3D object detection models usually take in LiDAR point clouds or multi-view images as input and aim to produce tight bounding boxes that describe nearby objects [9, 52, 26, 39, 40, 53, 54, 34]. Existing methods generally assume the supervised setting, in which the detector is trained with human-annotated bounding boxes. However, annotated data are often expensive to obtain

and limited in quantity. Furthermore, in tasks such as self-driving, environments can have highly varied conditions, and detectors with supervised training often require adaptation with additional labels from the new environment [47].

Unsupervised Object Discovery. The unsupervised object discovery task aims to identify and localize salient objects without learning from labels. Most existing works perform discovery from 2D images [8, 14, 45, 36, 2, 43, 48] or depth camera frames [21, 23, 17, 25, 20, 1]. Discovery from 3D LiDAR point clouds is underexplored. [49] performs joint unsupervised 2D detection and 3D instance segmentation from sequential point clouds and images based on temporal, motion and correspondence cues. MODEST [55] pioneers in performing label-free 3D object detection. It exploits high-level common sense properties from unlabeled data and bootstraps a dynamic object detector via repeated self-training. Despite promising performance, it requires excessive training time, which makes it difficult for practical use and development.

Reward Fine-Tuning for Model Alignment. Recently, foundation models [6, 29, 11, 44, 35, 37] have been shown to achieve strong performance in diverse tasks [5, 50], but sometimes produce outputs that do not align with human values [18, 30, 10]. A line of research aims to improve model alignment under the paradigm of Reinforcement Learning with Human Feedback (RLHF). Some pioneering works [41, 31, 33] learn a reward model and train foundation models with Proximal Policy Optimization (PPO) [38], but PPO is often expensive and unstable to train, and more importantly, requires a probabilistic output on the action space. This makes it hard to use for the object detection setting, which primarily uses regression-based losses. Reward ranked finetuning [27, 13] is a simplified alternative paradigm. It samples from a foundation model itself, filters generations using the reward model, and conducts supervised finetuning with the filtered generations.

3 Discovery from Reward-Incentivized Finetuning

Our framework, DRIFT, is inspired by the recent success of reward ranked finetuning methods for improving model alignment in the NLP community [13, 27]. We show that a similar approach can be adapted for 3D object discovery.

Problem Setup. We wish to obtain a dynamic object detection model on LiDAR data, i.e., a model to detect mobile objects in the LiDAR point clouds, *without human annotations*. Let $P \in \mathcal{R}^{N \times 3}$ denote a N-point 3D point cloud captured by LiDAR from which we wish to discover objects. We assume inputs of *unlabeled* point clouds collected by a car equipped with synchronized sensors including LiDAR (for point clouds) and GPS/INS (for accurate position and orientation). Since no annotation is involved, such a dataset is easy to acquire from daily driving routines; we additionally assume it to cover some locations with *multiple* scans at different times for computation of PP-score.

Dynamic Point Proposals. DRIFT leverages prior works that use unsupervised point clouds to extract foreground-background segmentation proposals. While many works [22, 3] have promising dynamic foreground segmentation results, in this work we rely on point *Persistency Prior score* (PP-score) [55] for its accuracy and leave the extension of other proposal methods to future work. For the purpose of this research, dynamic foreground points constitute LiDAR points reflecting off traffic participants (e.g. cars, bicyclists, pedestrians).

Using historical LiDAR sweeps collected at nearby locations of our point cloud P, the PP-score [3, 55] $\tau(P) \in [0,1]^N$ can provide an informative estimate on the per-point persistence, i.e., whether a point belongs to persistent background or not. The PP-score is defined as the normalized entropy over past point densities, based on the assumption that background space such as ground, trees, and buildings tend to exhibit consistent point densities across different LiDAR scans (high entropy), whereas points associated with mobile objects exhibit high density only if an object is present (low entropy).

3.1 Rewarding "Good" Dynamic Boxes

We first establish a reward function that evaluates the quality of a set of bounding boxes for dynamic objects in a scene. We denote a set of M dynamic objects bounding boxes as $\mathcal{B} = \{b_1, \ldots, b_M\}$, where each bounding box b_i is represented as an upright box with parameters $(x_i, y_i, z_i, w_i, l_i, h_i, \theta_i)$, defining the box's center, width, length, height, and z-rotation, respectively. The scoring function R scores the validity of the bounding boxes, given the observed point cloud P. In practice, a reward

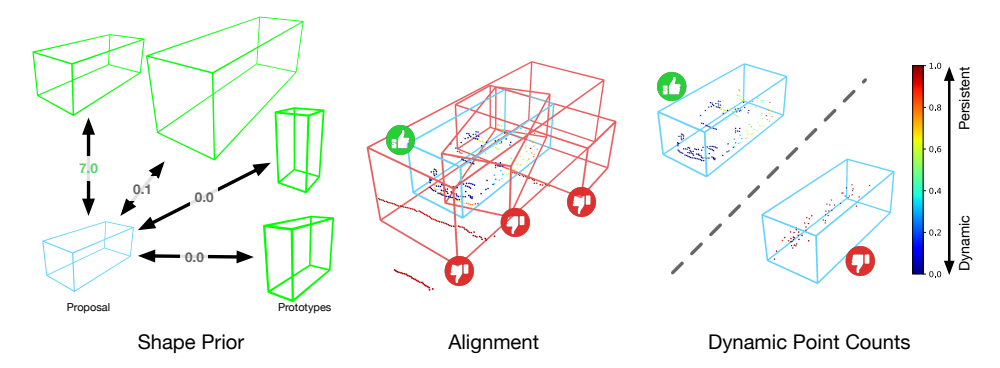


Figure 2: **Illustration of the reward components.** The reward encourages boxes that have proper shape and alignment, and capture more dynamic points and few background points.

function that is positively correlated with IoU should suffice. We present our proposed reward function which aims to capture only dynamic points, filter nonsensical boxes, enforce correct size, and encourage proper box alignment to the captured dynamic points.

Shape Prior Reward. We enforce a box to not deviate significantly from a set of prototype sizes $S = \{(\overline{w}_1, \overline{l}_1, \overline{h}_1), \dots, (\overline{w}_C, \overline{l}_C, \overline{h}_C)\}$ (Fig. 2 left). We assume the shape prior distribution is a mixture of C isotropic Gaussians with mixture weights π_i , diagonal variances Σ_i , and corresponding means as $(\overline{w}_i, \overline{l}_i, \overline{h}_i)$. These low-level statistics may be acquired directly from the dataset, or from vehicle specs and sales data available online [47]. In practice, we scale the mixtures such that the probabilities at the Gaussian means are equal for stability reasons. With this, the shape prior reward for box b is computed as:

$$R_{\text{shape}}(\boldsymbol{b}) = P_{\mathcal{S}}(\boldsymbol{b}). \tag{1}$$

Alignment Reward. Due to the nature of LiDAR sensing, the points will mostly fall on the lateral surfaces of an object. Therefore, a well-formed box should have dynamic points approximately close to the *boundary* of a box (Fig. 2 middle). As [55] shows, PP-score allows for easy separation of dynamic and persistent background points. Let $P_{\rm dyn}$ denote the set of dynamic points, and let $P_{\rm bg}$ be that of background points. In practice, since the PP-score is an approximation of ground-truth persistence, we define $P_{\rm dyn} = \{p|\tau(p) < 0.6\}$ and $P_{\rm bg} = \{p|\tau(p) \ge 0.9\}$.

Given a box b, we denote all points within and close to the box as $\mathcal{O}(b)$. Only points within $\mathcal{O}(b)$ contribute to the reward of b. In practice, we let $\mathcal{O}(b)$ consist of all points within a $\times 2$ scaled up version of b (with identical center and rotation). To score a box b, we design a reward function that identifies how "typical" the dynamic points within $\mathcal{O}(b)$ are. For each dynamic point $p \in \mathcal{O}(b) \cap P_{\rm dyn}$, we compute the scaling factor $s_{p,b}$ required so that the rescaled box touches p with one of its sides; i.e., if a point is inside the box, the box would have to be scaled down $(s_{p,b} < 1)$ to touch the point, if the point is outside it must be scaled up $(s_{p,b} > 1)$. We assume that $s_{p,b}$ roughly follows a Gaussian distribution centered near the box boundary, and visualize the actual distribution in Fig. 3.

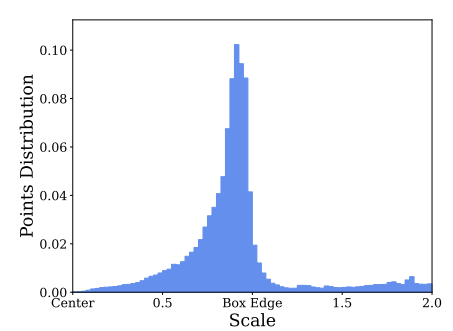


Figure 3: **Distribution of dynamic points** near ground truth bounding boxes. We observe that dynamic points near bounding boxes fall in an approximate Gaussian distribution centered near box edges $(s_{p,b} \approx 0.8)$.

We define our reward as the likelihood under this Gaussian distribution over scaling parameters. We approximate it as a Gaussian with hyper-parameters mean μ_{scale} and a variance σ_{scale} . Our reward is the product of the probability of each point in $\mathcal{O}(\boldsymbol{b})$:

$$R_{\text{align}}(\boldsymbol{b}) = \prod_{\boldsymbol{p} \in o(\boldsymbol{b}) \cap \boldsymbol{P}_{\text{dyn}}} \mathcal{N}(s_{\boldsymbol{p}, \boldsymbol{b}} | \mu_{\text{scale}}, \sigma_{\text{scale}}). \tag{2}$$

Common Sense Heuristics and Filtering. Lastly, a proper bounding box must capture the dynamic points, and avoid capturing the background points (Fig. 2, right). This heuristic can be encoded by a

simple weighted point count for each bounding box *b*:

$$R_{\text{count}}(\boldsymbol{b}) = \lambda_{\text{dyn}} \cdot |\boldsymbol{P}_{\text{dyn}} \cap \mathcal{O}(\boldsymbol{b})| - \lambda_{\text{bg}} \cdot |\boldsymbol{P}_{\text{bg}} \cap \mathcal{O}(\boldsymbol{b})|.$$

Intuitively, it assigns a reward in proportion to the number of dynamic points captured by the box, and a penalty in proportion to the number of background points captured.

Furthermore, boxes violating common sense should be assigned a low reward. We filter boxes that are too high up or too low from the ground, including those with too few dynamic points, or are too small or too large by directly assigning a reward of 0. In practice, we filter boxes that contain fewer than 4 dynamic points, or that have more than 80% persistent points, similar to [55].

In summary, the reward function is designed to be

$$R(\boldsymbol{b}) = \begin{cases} \lambda_{\text{shape}} \cdot R_{\text{shape}}(\boldsymbol{b}) + \lambda_{\text{align}} \cdot R_{\text{align}}(\boldsymbol{b}) + R_{\text{count}}(\boldsymbol{b}) & \text{if obeys common sense,} \\ 0 & \text{otherwise.} \end{cases}$$
(3)

3.2 Exploration Strategy for Improved Discovery

We assume a simple exploration strategy for identifying good box proposals. Given a set of current object proposals given by the detector, we locally perturb the boxes in the output space:

$$\mathcal{B}_{\text{explore}} \sim \mathcal{P}\left(\mathcal{B}_0, \sigma\right),$$
 (4)

where $\mathcal{B}_{\text{explore}}$ is the set of explored boxes, perturbed from the model proposals \mathcal{B}_0 . For each box $\mathbf{b} \in \mathcal{B}_0$, a set of explored boxes are sampled according to a standard Gaussian noise along the position and size dimensions and uniform noise for orientation:

$$b_{\text{explore}}^{\text{center}} \sim \mathcal{N}(b_0^{\text{center}}, \sigma^2 \mathbf{I}), \ b_{\text{explore}}^{\text{size}} \sim \mathcal{N}(b_0^{\text{size}}, \sigma^2 \mathbf{I}), \ b_{\text{explore}}^{\theta} \sim \mathcal{U}(b_0^{\theta} - \sigma, b_0^{\theta} + \sigma).$$
 (5)

Furthermore, to encourage proposals of boxes in foreground regions, we take inspiration from [56, 40] and re-use PP-score as *point-level* semantic segmentation (foreground vs background) labels, with which the detector is encouraged to propose boxes at points that have low PP-scores (i.e. are likely to be foreground points). Following [56], for each point $p_i \in P$ with prediction \hat{y}_i , we assign its target classification label y_i as:

$$y_{i} = \begin{cases} 1 & \text{if } \tau(p_{i}) < \tau_{L} \text{ or } \hat{y}_{i} = 1, \\ 0 & \text{otherwise.} \end{cases}$$
 (6)

Algorithm 1 Reward-Incentivized Finetuning

Input: Base object detector f_{θ} , unlabeled LiDAR dataset \mathcal{D} , exploration noise σ , sample size n, filter budget k, reward function R, PP-scores τ .

repeat

 $\begin{array}{ll} \boldsymbol{P} \sim \mathcal{D} & \rhd \text{ Sample point cloud.} \\ \mathcal{B}_0 \leftarrow f_{\theta}\left(\boldsymbol{P}\right) & \rhd \text{ Run detector for proposals.} \\ \mathcal{B}_{\text{explore}} \sim \mathcal{P}\left(\mathcal{B}_0, \sigma\right) & \rhd \text{ Sample } n \text{ boxes.} \\ \boldsymbol{r} \leftarrow \{R(\boldsymbol{b})\}_{\boldsymbol{b} \in \mathcal{B}_{\text{explore}} \cup \mathcal{B}_0} & \rhd \text{ Score boxes in set.} \\ \mathcal{B} \leftarrow \text{NMS}\left(\mathcal{B}_{\text{explore}} \cup \mathcal{B}_0, \boldsymbol{r}\right) \\ \mathcal{B}_{\text{top}} \leftarrow \text{Filter}(\mathcal{B}, \boldsymbol{r}, k) & \rhd \text{ Keep top } k\% \text{ boxes} \\ \text{Update } \theta \text{ with } \mathcal{B}_{\text{top}} \text{ for 1 step} \\ \textbf{until converged} \end{array}$

In effect, this encourages all non-persistent points (i.e., low $\tau(p_i)$) to propose boxes near dynamic regions for better exploration.

3.3 Reward-Incentivized Finetuning

The reward function R allows us to quickly evaluate proposed bounding boxes \mathcal{B} and the task of 3D object discovery could be reduced to an optimization problem on the total reward in box set space:

$$\mathcal{B}^* = \arg\max_{\mathcal{B}} \sum_{\boldsymbol{b} \in \mathcal{B}} R(\boldsymbol{b}), \tag{7}$$

where the sum is taken over the boxes in the set \mathcal{B} . Although a direct optimization for \mathcal{B}^* is not plausible due to the non-polynomial search space and discontinuity in R, R can serve as effective guidance to facilitate model finetuning. The underlying intuition is similar to curriculum learning [4, 28, 46]: the object detection model takes small steps to improve from its current predictions towards \mathcal{B}^* by following the direction provided by the maximum R direction in a local space.

As illustrated in Alg. 1, in each training iteration, we first let the object detector perform inference on a point cloud P and propose a set of dynamic objects \mathcal{B}_0 in the scene. To explore directions

of improvement with the non-differentiable reward function R, we sample n boxes from \mathcal{B}_0 (with replacement) and add an *i.i.d.* Gaussian noise on their location and size, and an uniform noise on orientation following Eq. 4. These sampled boxes are then ranked by the reward function R, in which the top k non-overlapping boxes are selected by Non-Maximum Suppression (NMS) as training targets to finetune the object detector. Note that since DRIFT treats the model training/inference procedures as black boxes, it can be applied to any 3D object detection model.

In practice, it is observed that neural networks can acquire task knowledge from imperfect demonstrations [16, 51, 32]. MODEST [55] pre-trained the 3D object detector on noisy seed labels produced by DBSCAN [15] clustering on spatial and PP-score. We follow [55] and initialize our 3D object detector a model trained with discovered seed labels.

4 Experiments

Datasets. We experimented with two different datasets: Lyft Level 5 Perception dataset [24] and Ithaca-365 dataset [12]. To the best of our knowledge, these are the two publicly available datasets that contain multiple traversals of multiple locations with accurate 6-DoF localization and 3D bounding box labels for traffic participants.

In the Lyft dataset, we experiment with the same split provided by [55], where the train set and test set are geographically separated. It consists of 11,873 train scenes and 4,901 test scenes. For the Ithaca365 dataset, we experimented with the full dataset which consists of 57,107 scenes for training and 1,644 for testing. For both datasets, we do not use any human-annotated labels in training. To show the generalizability of our method, we conduct the development on the Lyft dataset, i.e., all the hyperparameters of our approach are finalized through experiments on Lyft, and we use the exact same set of hyperparameters for all experiments in Ithaca365.

Evaluation. Following [55], we combine all traffic participants to a single mobile object class and evaluate the detector's performance on this class. Note that the labels are not used during training but solely for evaluation. For Lyft, we report the mean average precision (mAP) of the detector with the intersection over union (IoU) thresholds at 0.5 and 0.7 in bird-eye-view perspective. Note that mAP at 0.7 IoU threshold is a stricter and harder metric and was not evaluated in [55], and we include it to emphasize the effectiveness of our method. For Ithaca365, we adopt metrics similar to those in [7]: we evaluate mean average precision (mAP) for dynamic objects under $\{0.5, 1, 2, 4\}$ m thresholds that determine the match between detection and ground truth; we also compute 3 types of true positive metrics (TP metrics), including ATE, ASE and AOE for measuring translation, scale and orientation errors. These TP metrics are computed under a match distance threshold of 2m; additionally, we also compute a distance-based breakdown (0-30m, 30-50m, 50-80m) for these metrics.

Implementation. We use PointRCNN [40] as our default architecture and we use the implementation provided by OpenPCDet [42]. We train DRIFT with 120 epochs in Lyft and 30 epochs in Ithaca365 as the default setting, and observe that the performance generally improves with more training epochs (Fig. 1). We use $\lambda_{shape} = 1$, $\lambda_{align} = 1$, $\lambda_{dyn} = 0.001$ and $\lambda_{bg} = 0.001$. We use $\mu_{scale} = 0.8$ and $\sigma_{scale} = 0.2$ for the alignment reward. We define the shape priors based on four typical types of traffic participants: Car, Pedestrian, Cyclist, and Truck. Specifically, we use the mean and standard deviation of box sizes of each class in the Lyft dataset, but we show that they generalize well to other domains like Ithaca365 and are not sensitive (Tab. 2) The exact prototype sizes $\mathcal S$ and other implementation details can be found in the supplementary materials.

Baselines. To the best of our knowledge, MODEST [55] is the only prior work on this problem and we compare our method DRIFT against it with various variants of MODEST: (1) No Finetuning: the model trained with seed labels from PP-score without repeated self-training (MODEST (R0)) in [55]; (2) Self-Training (i ep): the model initialized with (1) and self-trained with i epochs without PP-score filtering; (3) MODEST (i ep): the model initialized with (1) and self-trained with i epochs with PP-score filtering (full MODEST model). For self-training in (2) and (3), we adopt 60 epochs for each self-training round in the Lyft dataset (same as that in [55]) and 30 epochs for the Ithaca365 dataset. To ensure a fair comparison, DRIFT is also initialized from (1) and use the same detector configurations as the baselines. Following [55], we also compare with the supervised counterparts trained with human-annotated labels from the same dataset (Lyft or Ithaca365) and from another out-of-domain dataset (KITTI).

Table 1: **Detection performance on Lyft.** DRIFT outperforms both baselines with 10% training time, and approaches the performance of the out-of-domain supervised detector trained on KITTI. Please refer to the setup of Sec. 4 for the metrics.

	n	nAP IoU	@ 0.5 (1	`)		mAP IoU @ 0.7 (†)				
Method	0-30	30-50	50-80	0-80	(0-30	30-50	50-80	0-80	
No Finetuning	44.1	21.1	1.2	23.9		24.4	6.0	0.1	10.5	
Self-Train. (60 ep) Self-Train. (600 ep) MODEST (60 ep) MODEST (600 ep) DRIFT (30 ep) DRIFT (60 ep) DRIFT (120 ep)	50.0 56.7 49.6 56.4 60.1 60.3 61.4	29.0 41.1 29.7 45.4 40.2 43.8 45.1	3.4 9.1 3.4 11.3 9.1 14.6 21.7	28.6 37.2 28.8 39.6 38.3 41.8 45.3		32.5 35.1 31.3 33.6 39.0 42.0 42.7	10.0 20.7 10.2 18.6 24.2 29.2 31.7	0.3 1.6 0.3 1.4 3.6 5.8 9.9	14.0 19.9 14.4 18.8 23.1 26.7 29.6	
Sup. on KITTI Sup. on Lyft	71.9 76.9	49.8 60.2	22.2 37.5	49.9 60.4		47.0 62.7	26.2 50.9	6.4 28.2	27.9 48.5	

Table 2: **Detection performance on Ithaca365.** We observe DRIFT outperforms both baselines with significantly less training time. Please refer to the setup of Sec. 4 for the metrics.

		mAP (†)					Errors 0-80m (↓)			
Method	0-30	30-50	50-80	0-80		ATE	ASE	AOE		
No Finetuning	18.7	4.8	0.0	7.7		1.17	0.60	1.64		
Self-Train. (30 ep) Self-Train. (300 ep) MODEST (30 ep) MODEST (300 ep) DRIFT (15 ep) DRIFT (30 ep)	25.9 16.3 14.6 27.5 39.1 47.1	9.2 3.6 0.7 26.3 24.3 31.2	1.2 1.8 0.0 21.0 17.7 22.9	12.4 6.8 3.7 27.1 28.0 35.1		1.08 1.19 0.83 1.06 0.73 0.49	0.62 0.74 0.52 0.67 0.33 0.35	1.57 1.57 1.53 1.09 1.23 1.20		
Sup. on KITTI Sup. on Ithaca365	59.8 75.7	28.3 48.3	4.0 22.6	32.0 51.5		0.26 0.18	0.22 0.13	0.46 0.33		

Dynamic Object Detection Results. We report the perfor- Table 3: Analysis on rewards of mance of DRIFT and baseline detectors on Lyft in Tab. 1, and show the performance over the training epochs in Fig. 1. We report the performance on Ithaca365 in Tab. 2. Notably, DRIFT demonstrates significantly faster learning and strong performance. It provides more than 10× speedup as compared to the baselines. On Lyft, DRIFT's performance at 60 epochs already surpasses the performance of both baselines at 600 epochs (10 self-training rounds) and approaches the performance of the out-of-domain supervised detector trained on KITTI [19]. On Ithaca365, its performance at 30 epochs significantly surpasses both baselines trained at 300 epochs. It even outperforms the out-of-domain supervised detector trained on KITTI in mAP.

boxes produced by different detectors. We report mean and std of box reward on the Lyft dataset.

Models	Mean	StD.
Rand. Boxes Self-Train. MODEST DRIFT	0.02 0.44 0.57 0.61	0.15 0.57 0.58 0.64
Ground Truth	1.00	0.42

Observe that the self-training performance starts collapsing with more rounds of self-training, and does not continue to improve.

Fig. 4 visualizes the detection on two scenes. Ground truth boxes are colored in green, predictions from the detector without fine-tuning are in yellow, and predictions from DRIFT are in red. We observe that the detector without fine-tuning occasionally produces false positive predictions, produces boxes with incorrect sizes, or misses moving objects, while DRIFT produces accurate detection.

Rewards ablations. We report the average reward per box for ground truth boxes, random boxes, and predicted boxes from different detectors in Tab. 3. The ground truth boxes have the highest rewards on average, while the random boxes have the lowest. This indicates that the reward reasonably reflects

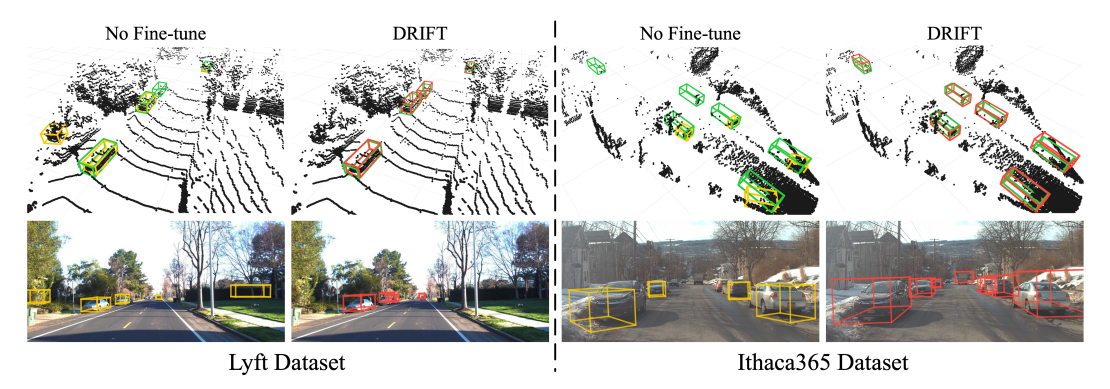


Figure 4: **Visualization of detections.** Qualitative results on two scenes from Lyft [24] and Ithaca365 [12] datasets. Ground truth boxes are labeled with green in the LiDAR figures and predictions without fine-tuning and DRIFT are in yellow and red, respectively. We observe DRIFT learns to produce accurate detection with correct shape and localization.

Table 4: Ablation on the reward components. We report the mAP (0-80m) on Lyft. Removing components significantly degrades performance.

Filter	Shape	Align.	mAP (0 - 80m)			
1 11001	Shape		IoU 0.5	IoU 0.7		
			0.6	0.0		
\checkmark	\checkmark		0.0	0.0		
	\checkmark	\checkmark	0.0	0.0		
\checkmark		\checkmark	22.4	3.2		
\checkmark	\checkmark	\checkmark	38.3	23.1		

Table 5: Ablation on the alignment reward's μ_{scale} . We report the mAP (0-80m) on the Lyft dataset. We show the detection performance is not sensitive to the choice of μ_{scale} .

μ_{scale}	mAP (0 - 80m)						
	IoU 0.5	IoU 0.7					
0.8	38.3	23.1					
0.9	38.1	23.4					

Table 6: Ablation on the alignment reward's σ_{scale} . We report the mAP (0-80m) on the Lyft dataset. The detection performance is not sensitive to the variance.

σ_{scale}	mAP (0 - 80m)						
	IoU 0.5	IoU 0.7					
0.1	34.2	20.9					
0.2	38.3	23.1					
0.3	38.1	20.0					
0.2	38.3	23.1					

the quality of the bounding box. And we observe the boxes predicted by DRIFT have higher rewards than those predicted by the baseline detectors.

Ablation study on the components of our reward is presented in Tab. 4, and visualization is shown in Fig. 5. Detection performance significantly drops when we remove one or more of the components. For example, when only common sense filtering is used, the detector just predicts boxes around foreground points. Without the shape prior reward, the detector predicts boxes with incorrect sizes.

Ablations Tab. 5 and Tab. 6 present the sensitivity analysis of the choices of μ_{scale} and σ_{scale} . DRIFT achieves stable performance across reasonable choices of μ_{scale} and σ_{scale} , showing the robustness of our method.

Exploration. We study the necessity of the exploration component and the effect of incorporating other sources for box sampling. In Tab. 7, we compare no exploration to: (1) sampling 200 boxes from box predictions, (2) sampling 100 from proposals near dynamic points and 100 from predictions, and (3) sampling 100 from seed labels and 100 from predictions. Observe that the exploration component is crucial for our method; by performing local exploration instead of simply updating from its own predictions, DRIFT avoids confirmation bias and ensures that labels improve over what it predicts. Furthermore, results show that sampling from the box predictions is sufficient for obtaining good performance; other sources do not provide obvious benefits.

We also explore the effects of modifying the exploration strategy. Tab. 8 compares the detector performance of using sample size of 50, 100 and 200, and noise scale σ (i.e. variation) of 0.3 vs. 0.6. Each detector is trained for 30 epochs. At noise scale 0.3, increasing the sample size from 50 to 200 significantly improves the detection performance. Using noise scale 0.6 significantly reduces the detection performance, indicating that smaller noise may be preferable.

Filtering Budget of the Ranked Boxes. We study the effect of the choice of top k% for filtering boxes by reward ranking. Tab. 9 presents the detection performance with top 55%, 65%, 75% and 85%. DRIFT is robust to the choice of k, with slightly decreased performance when k is too high.

Table 7: Detection performance with additional sampling sources in exploration. Sampling near the predictions is sufficient; additional sources do not provide obvious benefits. Trained for 60 ep.

		•			
	mAP (0 - 80m)				
	IoU 0.5	IoU 0.7			
No Exploration	0.0	0.0			
Sample near pred.	41.8	26.7			
+ near dynamic	39.3	22.6			
+ init. seed labels	39.5	22.8			

Table 8: Ablation on exploration parameters. Large sampling size and moderate noise scale are preferable.

Noise	Samples	mAP (0 - 80m)				
	Sumples	IoU 0.5	IoU 0.7			
0.3	50	32.9	14.3			
	100	36.4	18.9			
	200	38.3	23.1			
0.6	50	5.6	0.0			
	100	17.2	1.3			
	200	0.6	0.0			

Table 9: Ablation on the choice of top k% for box filtering by reward ranking. DRIFT is robust to different values of k.

Тор К	mAP (0 - 80m)						
	IoU 0.5	IoU 0.7					
55%	37.0	21.0					
65%	38.9	23.0					
75%	38.3	23.1					
85%	35.8	20.2					

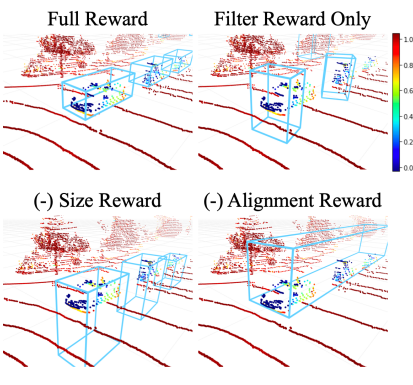


Figure 5: **Visualization of reward ablation.** Removing components leads to predictions with incorrect shape or position.

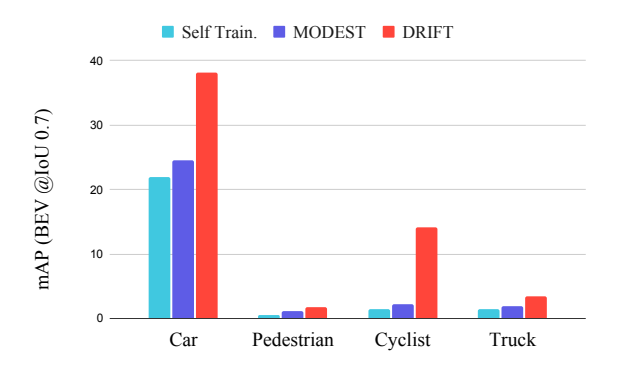


Figure 6: **Per-class BEV mAP at IoU 0.7.** We assign each predicted box to the class with the most similar prototype size. DRIFT outperforms the baselines for all classes.

Extension to Detection with Classes. Our prototype sizes are defined by different classes of traffic participants. Thus, given a predicted box from a class agnostic detector, we can compute the likelihood of its size under the Gaussian prior of each prototype size, and assign it to the class with the highest likelihood. Fig. 6 presents the per-class performance of DRIFT and baselines under such assignment. All detectors are trained for 60 epochs. DRIFT outperforms both baselines, with especially significant improvement for the Car and Cyclist classes. More details can be found in the supplementary materials.

5 Discussion and Conclusion

In this work, we propose a framework, DRIFT, to tackle object discovery without labels. Instead of requiring expensive 3D bounding box labels, our method utilizes succinctly described heuristics as a reward signal to initialize and subsequently fine-tune an object detector. To optimize this non-differentiable reward signal, we propose a simple but very effective reward finetuning framework, inspired by recent successes of reinforcement learning in the NLP community. Compared to prior self-training based methods [55], such a framework is an order of magnitude faster to train, while achieving higher accuracy. Traditional self-training iteratively generates pseudo-labels and retrains the model, requiring convergence before generating the next set of pseudo-labels. In general, training a detector to mimic pseudo-labels can lead to undesirable artifacts, further amplified by repeated training (confirmation bias). DRIFT addresses this issue by leveraging reinforcement learning principles, where the exploration component is crucial. Our method avoids confirmation bias by performing local exploration and ensures that labels improve over what it predicts. Thus, DRIFT is able to perform updates per-training iteration as opposed to per self-training round, which allows it to converge significantly faster and achieve higher performance.

Limitations and Future Works. One limitation is that the current framework is geared explicitly towards dynamic objects. Static objects would require different heuristics, not based on PP-scores. Similarly, currently we restricted our framework entirely to LiDAR signals. However, the reward

based framework is extremely flexible, and could easily be extended to other data modalities. For example, one could use image features to help identify objects inside of box proposals. Although in supervised settings image features have typically not added much in to the higher resolution LiDAR point clouds, in our unsupervised setting it is certainly possible that pixel information can help disambiguate objects from background. Further, we plan to explore the use of reward fine-tuning for other vision applications beyond object discovery.

Acknowledgments and Disclosure of Funding

This research is supported in part by grants from the National Science Foundation (III-2107161, IIS 2144117, and IIS-1724282), Nvidia Research, and DARPA Geometries of Learning (HR00112290078). We also thank Wei-Lun Chao, Yihong Sun, Travis Zhang, and Junan Chen for their valuable discussion.

References

- [1] Aikaterini Adam, Torsten Sattler, Konstantinos Karantzalos, and Tomas Pajdla. Objects can move: 3d change detection by geometric transformation consistency. In *Computer Vision–ECCV 2022: 17th European Conference, Tel Aviv, Israel, October 23–27, 2022, Proceedings, Part XXXIII*, pages 108–124. Springer, 2022. 3
- [2] Pablo Arbeláez, Jordi Pont-Tuset, Jonathan T Barron, Ferran Marques, and Jitendra Malik. Multiscale combinatorial grouping. In *Proceedings of the IEEE conference on computer vision and pattern recognition*, pages 328–335, 2014. 3
- [3] Dan Barnes, Will Maddern, Geoffrey Pascoe, and Ingmar Posner. Driven to distraction: Self-supervised distractor learning for robust monocular visual odometry in urban environments. In 2018 IEEE International Conference on Robotics and Automation (ICRA), pages 1894–1900. IEEE, 2018. 2, 3
- [4] Yoshua Bengio, Jérôme Louradour, Ronan Collobert, and Jason Weston. Curriculum learning. In *Proceedings of the 26th annual international conference on machine learning*, pages 41–48, 2009. 5
- [5] Rishi Bommasani, Drew A Hudson, Ehsan Adeli, Russ Altman, Simran Arora, Sydney von Arx, Michael S Bernstein, Jeannette Bohg, Antoine Bosselut, Emma Brunskill, et al. On the opportunities and risks of foundation models. *arXiv preprint arXiv:2108.07258*, 2021. 3
- [6] Tom Brown, Benjamin Mann, Nick Ryder, Melanie Subbiah, Jared D Kaplan, Prafulla Dhariwal, Arvind Neelakantan, Pranav Shyam, Girish Sastry, Amanda Askell, et al. Language models are few-shot learners. *Advances in neural information processing systems*, 33:1877–1901, 2020. 3
- [7] Holger Caesar, Varun Bankiti, Alex H Lang, Sourabh Vora, Venice Erin Liong, Qiang Xu, Anush Krishnan, Yu Pan, Giancarlo Baldan, and Oscar Beijbom. nuscenes: A multimodal dataset for autonomous driving. In CVPR, pages 11621–11631, 2020. 6
- [8] Joao Carreira and Cristian Sminchisescu. Constrained parametric min-cuts for automatic object segmentation. In 2010 IEEE Computer Society Conference on Computer Vision and Pattern Recognition, pages 3241–3248. IEEE, 2010. 3
- [9] Xiaozhi Chen, Huimin Ma, Ji Wan, Bo Li, and Tian Xia. Multi-view 3d object detection network for autonomous driving. In *Proceedings of the IEEE conference on Computer Vision and Pattern Recognition*, pages 1907–1915, 2017. 2
- [10] Jaemin Cho, Abhay Zala, and Mohit Bansal. Dall-eval: Probing the reasoning skills and social biases of text-to-image generative transformers. arXiv preprint arXiv:2202.04053, 2022.
- [11] Aakanksha Chowdhery, Sharan Narang, Jacob Devlin, Maarten Bosma, Gaurav Mishra, Adam Roberts, Paul Barham, Hyung Won Chung, Charles Sutton, Sebastian Gehrmann, et al. Palm: Scaling language modeling with pathways. *arXiv preprint arXiv:2204.02311*, 2022. 3
- [12] Carlos A Diaz-Ruiz, Youya Xia, Yurong You, Jose Nino, Junan Chen, Josephine Monica, Xiangyu Chen, Katie Luo, Yan Wang, Marc Emond, et al. Ithaca365: Dataset and driving perception under repeated and challenging weather conditions. In *Proceedings of the IEEE/CVF Conference on Computer Vision and Pattern Recognition*, pages 21383–21392, 2022. 2, 6, 8

- [13] Hanze Dong, Wei Xiong, Deepanshu Goyal, Rui Pan, Shizhe Diao, Jipeng Zhang, Kashun Shum, and Tong Zhang. Raft: Reward ranked finetuning for generative foundation model alignment. *arXiv preprint arXiv:2304.06767*, 2023. 2, 3
- [14] Ian Endres and Derek Hoiem. Category independent object proposals. In *ECCV* (5), pages 575–588. Citeseer, 2010. 3
- [15] Martin Ester, Hans-Peter Kriegel, Jörg Sander, Xiaowei Xu, et al. A density-based algorithm for discovering clusters in large spatial databases with noise. In *kdd*, volume 96, pages 226–231, 1996. 6
- [16] Yang Gao, Huazhe Xu, Ji Lin, Fisher Yu, Sergey Levine, and Trevor Darrell. Reinforcement learning from imperfect demonstrations. corr abs/1802.05313 (2018). arXiv preprint arXiv:1802.05313, 1802. 6
- [17] Germán M García, Ekaterina Potapova, Thomas Werner, Michael Zillich, Markus Vincze, and Simone Frintrop. Saliency-based object discovery on rgb-d data with a late-fusion approach. In 2015 IEEE International Conference on Robotics and Automation (ICRA), pages 1866–1873. IEEE, 2015. 3
- [18] Samuel Gehman, Suchin Gururangan, Maarten Sap, Yejin Choi, and Noah A Smith. Realtoxicityprompts: Evaluating neural toxic degeneration in language models. *arXiv preprint arXiv:2009.11462*, 2020. 3
- [19] Andreas Geiger, Philip Lenz, Christoph Stiller, and Raquel Urtasun. Vision meets robotics: The kitti dataset. *The International Journal of Robotics Research*, 32(11):1231–1237, 2013. 7
- [20] Maciej Halber, Yifei Shi, Kai Xu, and Thomas Funkhouser. Rescan: Inductive instance segmentation for indoor rgbd scans. In *Proceedings of the IEEE/CVF International Conference on Computer Vision*, pages 2541–2550, 2019. 3
- [21] Evan Herbst, Xiaofeng Ren, and Dieter Fox. Rgb-d object discovery via multi-scene analysis. In 2011 IEEE/RSJ International Conference on Intelligent Robots and Systems, pages 4850–4856. IEEE, 2011. 3
- [22] Xiangru Huang, Yue Wang, Vitor Guizilini, Rares Ambrus, Adrien Gaidon, and Justin Solomon. Representation learning for object detection from unlabeled point cloud sequences. In *Conference on Robot Learning*, 2022. 3
- [23] Andrej Karpathy, Stephen Miller, and Li Fei-Fei. Object discovery in 3d scenes via shape analysis. In 2013 IEEE international conference on robotics and automation, pages 2088–2095. IEEE, 2013. 3
- [24] R. Kesten, M. Usman, J. Houston, T. Pandya, K. Nadhamuni, A. Ferreira, M. Yuan, B. Low, A. Jain, P. Ondruska, S. Omari, S. Shah, A. Kulkarni, A. Kazakova, C. Tao, L. Platinsky, W. Jiang, and V. Shet. Lyft level 5 av dataset 2019. urlhttps://level5.lyft.com/dataset/, 2019. 2, 6, 8
- [25] Deyvid Kochanov, Aljoša Ošep, Jörg Stückler, and Bastian Leibe. Scene flow propagation for semantic mapping and object discovery in dynamic street scenes. In 2016 IEEE/RSJ International Conference on Intelligent Robots and Systems (IROS), pages 1785–1792. IEEE, 2016. 3
- [26] Alex H Lang, Sourabh Vora, Holger Caesar, Lubing Zhou, Jiong Yang, and Oscar Beijbom. Pointpillars: Fast encoders for object detection from point clouds. In *Proceedings of the IEEE/CVF conference on computer vision and pattern recognition*, pages 12697–12705, 2019.
- [27] Ximing Lu, Sean Welleck, Jack Hessel, Liwei Jiang, Lianhui Qin, Peter West, Prithviraj Ammanabrolu, and Yejin Choi. Quark: Controllable text generation with reinforced unlearning. Advances in neural information processing systems, 35:27591–27609, 2022. 2, 3
- [28] Sanmit Narvekar, Bei Peng, Matteo Leonetti, Jivko Sinapov, Matthew E Taylor, and Peter Stone. Curriculum learning for reinforcement learning domains: A framework and survey. *The Journal of Machine Learning Research*, 21(1):7382–7431, 2020. 5
- [29] OpenAI. Gpt-4 technical report, 2023. 3
- [30] Nedjma Ousidhoum, Xinran Zhao, Tianqing Fang, Yangqiu Song, and Dit-Yan Yeung. Probing toxic content in large pre-trained language models. In *Proceedings of the 59th Annual Meeting of the Association for Computational Linguistics and the 11th International Joint Conference on Natural Language Processing (Volume 1: Long Papers)*, pages 4262–4274, 2021. 3
- [31] Long Ouyang, Jeffrey Wu, Xu Jiang, Diogo Almeida, Carroll Wainwright, Pamela Mishkin, Chong Zhang, Sandhini Agarwal, Katarina Slama, Alex Ray, et al. Training language models to follow instructions with human feedback. *Advances in Neural Information Processing Systems*, 35:27730–27744, 2022. 2, 3

- [32] Deepak Pathak, Ross Girshick, Piotr Dollár, Trevor Darrell, and Bharath Hariharan. Learning features by watching objects move. In *Proceedings of the IEEE conference on computer vision and pattern recognition*, pages 2701–2710, 2017. 6
- [33] André Susano Pinto, Alexander Kolesnikov, Yuge Shi, Lucas Beyer, and Xiaohua Zhai. Tuning computer vision models with task rewards. arXiv preprint arXiv:2302.08242, 2023. 2, 3
- [34] Charles R Qi, Or Litany, Kaiming He, and Leonidas J Guibas. Deep hough voting for 3d object detection in point clouds. In *proceedings of the IEEE/CVF International Conference on Computer Vision*, pages 9277–9286, 2019. 2
- [35] Aditya Ramesh, Mikhail Pavlov, Gabriel Goh, Scott Gray, Chelsea Voss, Alec Radford, Mark Chen, and Ilya Sutskever. Zero-shot text-to-image generation. In *International Conference on Machine Learning*, pages 8821–8831. PMLR, 2021. 3
- [36] Zhile Ren and Gregory Shakhnarovich. Image segmentation by cascaded region agglomeration. In Proceedings of the IEEE Conference on Computer Vision and Pattern Recognition, pages 2011–2018, 2013.
 3
- [37] Robin Rombach, Andreas Blattmann, Dominik Lorenz, Patrick Esser, and Björn Ommer. High-resolution image synthesis with latent diffusion models. In *Proceedings of the IEEE/CVF Conference on Computer Vision and Pattern Recognition*, pages 10684–10695, 2022. 3
- [38] John Schulman, Filip Wolski, Prafulla Dhariwal, Alec Radford, and Oleg Klimov. Proximal policy optimization algorithms. arXiv preprint arXiv:1707.06347, 2017. 3
- [39] Shaoshuai Shi, Chaoxu Guo, Li Jiang, Zhe Wang, Jianping Shi, Xiaogang Wang, and Hongsheng Li. Pv-rcnn: Point-voxel feature set abstraction for 3d object detection. In *Proceedings of the IEEE/CVF Conference on Computer Vision and Pattern Recognition*, pages 10529–10538, 2020. 2
- [40] Shaoshuai Shi, Xiaogang Wang, and Hongsheng Li. Pointrenn: 3d object proposal generation and detection from point cloud. In *Proceedings of the IEEE/CVF conference on computer vision and pattern recognition*, pages 770–779, 2019. 1, 2, 5, 6
- [41] Nisan Stiennon, Long Ouyang, Jeffrey Wu, Daniel Ziegler, Ryan Lowe, Chelsea Voss, Alec Radford, Dario Amodei, and Paul F Christiano. Learning to summarize with human feedback. *Advances in Neural Information Processing Systems*, 33:3008–3021, 2020. 3
- [42] OpenPCDet Development Team. Openpcdet: An open-source toolbox for 3d object detection clouds. https://github.com/open-mmlab/OpenPCDet, 2020. 6
- [43] Hao Tian, Yuntao Chen, Jifeng Dai, Zhaoxiang Zhang, and Xizhou Zhu. Unsupervised object detection with lidar clues. In *Proceedings of the IEEE/CVF Conference on Computer Vision and Pattern Recognition*, pages 5962–5972, 2021. 3
- [44] Hugo Touvron, Thibaut Lavril, Gautier Izacard, Xavier Martinet, Marie-Anne Lachaux, Timothée Lacroix, Baptiste Rozière, Naman Goyal, Eric Hambro, Faisal Azhar, et al. Llama: Open and efficient foundation language models. arXiv preprint arXiv:2302.13971, 2023. 3
- [45] Jasper RR Uijlings, Koen EA Van De Sande, Theo Gevers, and Arnold WM Smeulders. Selective search for object recognition. *International journal of computer vision*, 104:154–171, 2013. 3
- [46] Chen Wang, Junfeng Ding, Xiangyu Chen, Zelin Ye, Jialu Wang, Ziruo Cai, and Cewu Lu. Tendencyrl: Multi-stage discriminative hints for efficient goal-oriented reverse curriculum learning. In 2019 IEEE/RSJ International Conference on Intelligent Robots and Systems (IROS), pages 3474–3480. IEEE, 2019. 5
- [47] Yan Wang, Xiangyu Chen, Yurong You, Li Erran Li, Bharath Hariharan, Mark Campbell, Kilian Q Weinberger, and Wei-Lun Chao. Train in germany, test in the usa: Making 3d object detectors generalize. In Proceedings of the IEEE/CVF Conference on Computer Vision and Pattern Recognition, pages 11713–11723, 2020. 3, 4
- [48] Yangtao Wang, Xi Shen, Shell Xu Hu, Yuan Yuan, James L Crowley, and Dominique Vaufreydaz. Self-supervised transformers for unsupervised object discovery using normalized cut. In *Proceedings of the IEEE/CVF Conference on Computer Vision and Pattern Recognition*, pages 14543–14553, 2022. 3
- [49] Yuqi Wang, Yuntao Chen, and Zhaoxiang Zhang. 4d unsupervised object discovery. *arXiv preprint* arXiv:2210.04801, 2022. 3

- [50] Jason Wei, Yi Tay, Rishi Bommasani, Colin Raffel, Barret Zoph, Sebastian Borgeaud, Dani Yogatama, Maarten Bosma, Denny Zhou, Donald Metzler, et al. Emergent abilities of large language models. arXiv preprint arXiv:2206.07682, 2022. 3
- [51] Yueh-Hua Wu, Nontawat Charoenphakdee, Han Bao, Voot Tangkaratt, and Masashi Sugiyama. Imitation learning from imperfect demonstration. In *International Conference on Machine Learning*, pages 6818–6827. PMLR, 2019. 6
- [52] Yan Yan, Yuxing Mao, and Bo Li. Second: Sparsely embedded convolutional detection. *Sensors*, 18(10):3337, 2018. 2
- [53] Zetong Yang, Yanan Sun, Shu Liu, and Jiaya Jia. 3dssd: Point-based 3d single stage object detector. In Proceedings of the IEEE/CVF conference on computer vision and pattern recognition, pages 11040–11048, 2020. 2
- [54] Zetong Yang, Yanan Sun, Shu Liu, Xiaoyong Shen, and Jiaya Jia. Std: Sparse-to-dense 3d object detector for point cloud. In *Proceedings of the IEEE/CVF international conference on computer vision*, pages 1951–1960, 2019. 2
- [55] Yurong You, Katie Luo, Cheng Perng Phoo, Wei-Lun Chao, Wen Sun, Bharath Hariharan, Mark Campbell, and Kilian Q Weinberger. Learning to detect mobile objects from lidar scans without labels. In *Proceedings of the IEEE/CVF Conference on Computer Vision and Pattern Recognition*, pages 1130–1140, 2022. 1, 2, 3, 4, 5, 6, 9
- [56] Yurong You, Cheng Perng Phoo, Katie Luo, Travis Zhang, Wei-Lun Chao, Bharath Hariharan, Mark Campbell, and Kilian Q Weinberger. Unsupervised adaptation from repeated traversals for autonomous driving. Advances in Neural Information Processing Systems, 35:27716–27729, 2022. 5

Supplementary Material: Reward Finetuning for Faster and More Accurate Unsupervised Object Discovery

S1 Additional Implementation Details

We train DRIFT on four NVIDIA RTX A6000 GPUs, with batch size 10 per GPU. The values we use for the shape priors are reported in Tab. S10. In practice, we scale the mixtures such that the probabilities at the Gaussian means are equal for stability reasons. The values in Tab. S10 are computed from the box shapes in the Lyft dataset, but the method generalize well to other domains like Ithaca365. Bear in mind, all models trained on Ithaca365 directly uses the hyperparameters found in Lyft, suggesting the generalizability of our method. DRIFT achieves stable performance when alternative values are used (Tab. S16).

Mixture Component	Width w		Len	gth l	Height h		
	Mean	StD.	Mean	StD.	Mean	StD.	
1 (Car)	1.911	0.162	4.745	0.559	1.711	0.248	
2 (Pedestrian)	0.780	0.153	0.797	0.182	1.745	0.177	
3 (Truck)	2.832	0.278	9.403	3.145	3.299	0.430	
4 (Cyclist)	0.613	0.256	1.752	0.326	1.364	0.343	

Table S10: Shape prior values used in our implementation.

S2 Extended Quantitative Results

S2.1 Full Tables from Main Paper

We provide results on all ranges for all ablation tables shown in the the main paper. In Tab. S11, we report the results of the alignment reward ablation on μ_{scale} . In Tab. S12, we report ablation results on reward components. In Tab. S13 and Tab. S14 we report ablation on exploration method and sample counts, respectively. In Tab. S15, we report ablation results for varying the filter budget.

Table S11: Ablation on the alignment reward's μ_{scale} . We report the mAP (0-80m) on the Lyft dataset. This corresponds with Table 5 of the main paper.

Alignment Reward	mAP IoU 0.5				mAP IoU 0.7				
	0-30	30-50	50-80	0-80	0-30	30-50	50-80	0-80	
$\mu = 0.8$ $\mu = 0.9$			9.1 10.1	38.3 38.1	39.0 37.1	24.2 26.0	3.6 4.4	23.1 23.4	

S2.2 Ablation on Shape Prior Reward

We additionally include an ablation study on the shape-prior reward in Tab. S16. We show that it is not sensitive to the choice in variance used for each class. We assume that the means of the shape priors are user defined.

S2.3 Lower IoU and Recall Evaluation

We report mAP results at IoU 0.25 match in Tab. S17. In particular, IoU 0.25 metric evaluates "localization", i.e. if there is a bounding box with a very small overlap with the ground truth. However,

Table S12: Ablation on the reward components. We report the mAP (0-80m) on the Lyft dataset. This table corresponds to Table 4 in the main paper.

			mAP IoU 0.5					mAP Io	U 0.7	
Filtering	Size Prior	Align.	0-30	30-50	50-80	0-80	0-30	30-50	50-80	0-80
√			1.3	0.8	0.0	0.6	0.0	0.0	0.0	0.0
\checkmark	\checkmark		0.0	0.0	0.0	0.0	0.0	0.0	0.0	0.0
	\checkmark	\checkmark	0.0	0.0	0.0	0.0	0.0	0.0	0.0	0.0
\checkmark		\checkmark	41.2	18.2	1.7	22.4	5.3	5.0	0.3	3.2
\checkmark	\checkmark	\checkmark	60.1	40.2	9.1	38.3	39.0	24.2	3.6	23.1

Table S13: Detection performance with additional sampling sources in exploration. Sampling near the predictions is sufficient; additional sources do not provide obvious benefits.

	mAP IoU 0.5				mAP IoU 0.7				
	0-30	30-50	50-80	0-80	0-30	30-50	50-80	0-80	
Sample near pred. + near dynamic + init. seed labels	60.3 59.8 60.3	43.8 40.9 40.7	14.6 10.6 10.4	41.8 39.3 39.5	42.0 39.1 38.4	29.2 22.8 23.9	5.8 3.2 3.3	26.7 22.6 22.8	

our method excels at predicting the size and proper orientation, which is better captured at higher IoUs metrics. To summarize, as compared to the prior work, MODEST can localize boxes well, but it's not able to figure out the size; in contrast, our method does both well. As stated in the main paper, we use 0.5 and 0.7 to (1) following the KITTI and Lyft standards of reporting, and (2) emphasize the strength of our method.

In addition, we report recall metrics in Tab. S18. We see that the recall improves over additional training, which suggests that part of the improvement comes from being able to better detect bounding boxes by locating them in the scene.

S2.4 Ablation on class mixtures

We include additional experiments on the class type mixtures that we use in the reward function of DRIFT to evaluate the robustness of our method. We report the results of using 4 (the ground truth number), 5, and 6 factors in the Gaussian mixture in Tab. S19.

S3 Extended Qualitative Visualizations

We showcase additional qualitative results in Fig. S8. Observe that DRIFT improves significantly over the model without fine-tuning, and close to supervised performance, without any labels.

Table S18: **Recall by epoch.** We report class recall numbers at different training epochs. Observe that DRIFT training improves the recall.

Epoch	Recall (0 - 80m)						
_potii	IoU 0.5	IoU 0.7					
30	0.47	0.30					
60	0.51	0.34					
90	0.53	0.36					
120	0.56	0.38					

Table S14: Ablation on sampling hyperparameters for exploration. Large sampling size and moderate noise scale are preferable.

			mAP IoU 0.5					mAP Io	U 0.7	
Noise	Samples	0-30	30-50	50-80	0-80		0-30	30-50	50-80	0-80
	50	57.3	31.3	4.8	32.9		26.0	14.4	1.4	14.3
0.3	100	59.8	36.2	7.0	36.4		33.0	18.9	1.8	18.9
	200	60.1	40.2	9.1	38.3		39.0	24.2	3.6	23.1
	50	17.8	1.2	0.0	5.6		0.1	0.0	0.0	0.0
0.6	100	39.5	10.4	0.2	17.2		4.0	0.3	0.0	1.3
	200	0.1	0.9	1.1	0.6		0.0	0.0	0.0	0.0

Table S15: Ablation on the choice of top k% for box filtering by reward ranking. DRIFT is robust to different values of k.

Top $k\%$		mAP I	oU 0.5			mAP IoU 0.7				
10p 1070	0-30	30-50	50-80	0-80	0-30	30-50	50-80	0-80		
55%	60.0	36.5	7.5	37.0	36.5	20.1	2.3	21.0		
65%	60.1	39.9	9.7	38.9	39.1	23.4	3.5	23.0		
75%	60.1	40.2	9.1	38.3	39.0	24.2	3.6	23.1		
85%	58.1	36.6	6.6	35.8	35.8	20.6	2.3	20.2		

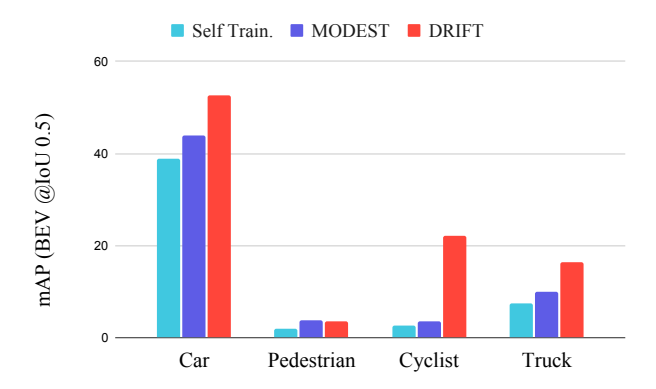


Figure S7: **Per-class BEV mAP at IoU 0.5.** We assign each predicted box to the class with the most similar prototype size. This corresponds to Figure 6 of the main paper.

Table S16: Ablation on variance of the class shape priors.

Class Shape Var.		mAP I	oU 0.5		mAP IoU 0.7			
	0-30	30-50	50-80	0-80	0-30	30-50	50-80	0-80
$\sigma_i = 0.5$ StD.	57.6	34.5	5.1	34.5	36.8	22.5	1.7	21.3
$\sigma_i = 0.2$ StD.	55.3	40.2	11.1	37.1	39.8	27.9	5.2	25.5
True Variance	60.1	40.2	9.1	38.3	39.0	24.2	3.6	23.1

Table S17: **Detection performance on the Lyft dataset.** We report the evaluation results at IoU 0.25. This metric is evaluating "localization", i.e. if there is a bounding box with a tiny overlap with the GT. Our method matches the baselines on this match threshold, and surpasses on the more strict IoU thresholds of 0.5 and 0.7.

	r	nAP IoU	0.25 (†)	
	0-30	30-50	50-80	0-80
No Finetuning	63.5	34.9	6.0	37.5
Self-Train. (60 ep)	67.7	43.2	8.7	43.1
Self-Train. (600 ep)	67.7	48.0	13.3	45.5
MODEST (60 ep)	68.5	46.2	10.5	45.1
MODEST (600 ep)	73.6	56.8	21.0	53.6
DRIFT (60ep)	72.3	51.5	19.2	50.7
DRIFT (120 ep)	72.5	51.7	25.8	52.9
Supervised on KITTI Supervised on Lyft	78.6 81.8	53.9 63.6	26.1 40.0	55.3 64.2

Table S19: **Ablation on the number of factors in the class mixture.** We test out additional class sizes other than the ground truth number of classes in the label set (car, pedestrian, cyclist, truck). Observe that the number of factors does not significantly affect the performance of DRIFT.

	mAP IoU 0.5					mAP IoU 0.7					
Num. Factors	0-30	30-50	50-80	0-80	-	0-30	30-50	50-80	0-80		
4 (GT)	60.1	40.2	9.1	38.3		39.0	24.2	3.6	23.1		
5	59.8	37.9	7.4	37.0		38.6	24.7	2.9	23.0		
6	58.5	38.3	6.1	36.0		39.1	23.9	2.6	22.7		

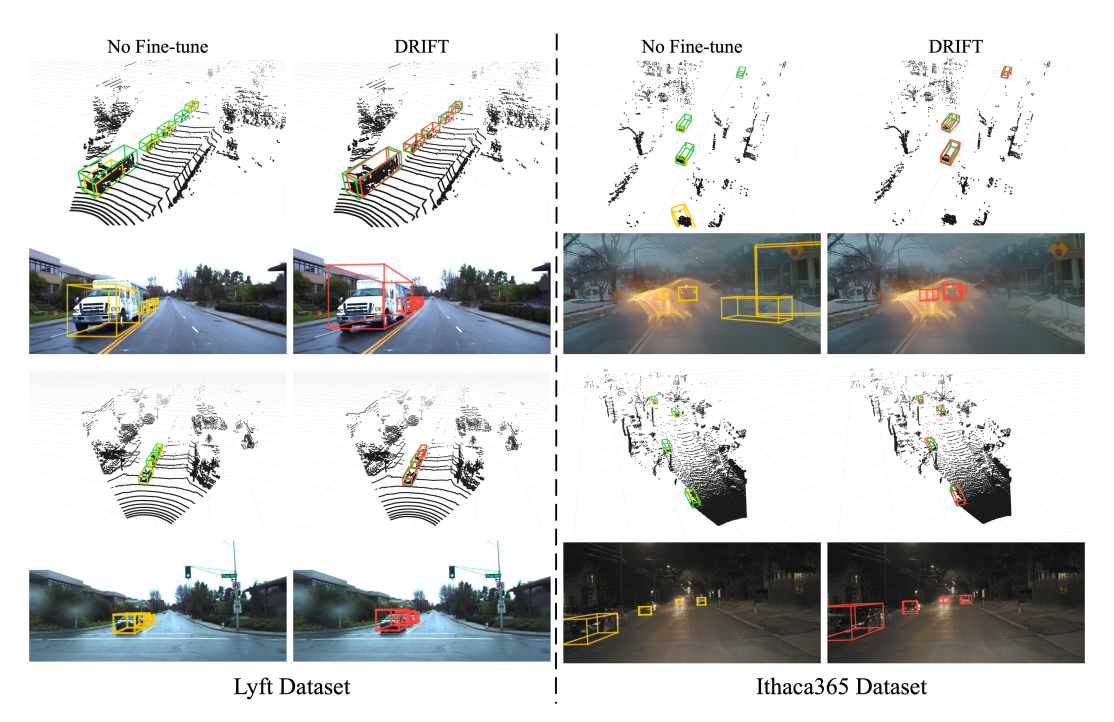


Figure S8: **Qualitative visualizations.** Additional visualizations of the DRIFT method, as compared to no fine-tuning.